Spectroscopy of the neutron-deficient $N = 50$ nucleus ^{95}Rh

F. Ghazi Moradi,[1,*] B. Cederwall,[1] C. Qi,[1] T. Bäck,[1] A. Ataç,[1,†] R. Liotta,[1] M. Doncel,[1] A. Johnson,[1] G. de France,[2]
E. Clément,[2] J. Nyberg,[3] A. Gengelbach,[3] B. M. Nyakó,[4] J. Gál,[4] G. Kalinka,[4] J. Molnár,[4] J. Timár,[4] D. Sohler,[4] Zs. Dombrádi,[4]
I. Kuti,[4] K. Juhász,[5,‡] D. R. Napoli,[6] A. Gottardo,[6] V. Modamio,[6] R. Wadsworth,[7] T. W. Henry,[7] A. J. Nichols,[7] H. Al-Azri,[7]
M. Palacz,[8] E. Ideguchi,[9] Ö. Aktas,[10,11] A. Di Nitto,[12,§] A. Dijon,[2] T. Hüyük,[13] G. Jaworski,[14,8] P. R. John,[15] and B. Yilmaz[16]

[1]*Department of Physics, Royal Institute of Technology (KTH), SE-10691 Stockholm, Sweden*
[2]*Grand Accélérateur National d'Ions Lourds (GANIL), CEA/DSM–CNRS/IN2P3, F-14076 Caen Cedex 5, France*
[3]*Department of Physics and Astronomy, Uppsala University, SE-75121 Uppsala, Sweden*
[4]*MTA Atomki, H-4001 Debrecen, Hungary*
[5]*Department of Information Technology, University of Debrecen, H-4032 Debrecen, Hungary*
[6]*Istituto Nazionale di Fisica Nucleare, Laboratori Nazionali di Legnaro, I-35020 Legnaro, Italy*
[7]*Department of Physics, University of York, YO10 5DD York, United Kingdom*
[8]*Heavy Ion Laboratory, University of Warsaw, 02-093 Warsaw, Poland*
[9]*Research Center for Nuclear Physics, Osaka University, Ibaraki, 567-0047 Osaka, Japan*
[10]*Department of Physics, Middle East Technical University, 06531 Ankara, Turkey*
[11]*Department of Physics, Necmettin Erbakan University, 42090 Konya, Turkey*
[12]*Istituto Nazionale di Fisica Nucleare, Sezione di Napoli, I-80126 Napoli, Italy*
[13]*Instituto de Física Corpuscular, CSIC-Universitat de València, E-46980 València, Spain*
[14]*Faculty of Physics, Warsaw University of Technology, 00-662 Warsaw, Poland*
[15]*Dipartimento di Fisica e Astronomia, Università di Padova, and Istituto Nazionale di Fisica Nucleare,
Sezione di Padova, I-35131 Padua, Italy*
[16]*Department of Physics, Ankara University, 06100 Tandoğan, Ankara, Turkey*

The neutron-deficient semimagic (neutron number $N = 50$) ^{95}Rh nucleus has been produced at high spins using the projectile-target system ^{40}Ca $+^{58}$Ni at 125 MeV beam energy. The γ-decays of levels populated by the $3p$ fusion evaporation reaction channel were studied using γ-γ coincidences, and 20 new γ-ray transitions involving 15 new positive- and negative-parity states were observed. Spin and parity for many of the excited states were firmly deduced for the first time using the combined directional angular correlation and direction-polarization techniques. The observed structures are discussed within the framework of large-scale shell model calculations. $E1$ transition strengths were deduced and used together with the results of the shell model calculations to study the contribution of different particle-hole configurations, in particular for analyzing contributions from core-excited configurations.

PACS number(s): 21.10.Re, 23.20.Lv, 25.70.−z, 27.60.+j

I. INTRODUCTION

The structural evolution along the $N = 50$ ($Z = 50$) isotonic (isotopic) chains, approaching the double shell closure, is of key interest in current nuclear structure physics. Indeed, atomic nuclei near the presumed doubly magic nucleus ^{100}Sn have attracted the attention of numerous theoretical and experimental studies in recent years (see for example [1] and references therein). The structure of the low-lying states in nuclei just below ^{100}Sn can be rather well described within a simple model space including the shells $0g_{9/2}$ and $1p_{1/2}$. One question of particular importance is the role played by excitations crossing the $N = Z = 50$ shell closure. Core-excited states have been observed in semimagic nuclei including

^{93}Tc, ^{94}Ru, ^{95}Rh, ^{96}Pd, ^{97}Ag, and ^{98}Cd [2–5]. Moreover, neutron-proton (np) correlations can be expected to play an increasing role, as the valence nucleons occupy identical orbits. As a result, the standard seniority isovector structures may be subject to competition from a new, isoscalar neutron-proton pair-coupling scheme in the $N \approx Z$ nuclei [6,7]. In the present study we have investigated the structure of $^{95}_{45}$Rh$_{50}$ and the validity of its representation in terms of different seniority configurations using large-scale shell model (LSSM) calculations. We here present new polarization and angular correlation measurements of γ rays in ^{95}Rh which enabled us to deduce parities and angular momenta of nuclear states up to spin $>20\hbar$. The previously reported level scheme was revised and extended. The strengths of forbidden $E1$ transitions have been extracted from branching ratios and previously measured lifetimes [8] and were used to test the LSSM predictions.

II. EXPERIMENTAL DETAILS

Excited states in ^{95}Rh were observed following the heavy-ion fusion evaporation reaction ^{58}Ni(^{40}Ca,$3p$)^{95}Rh at a beam

---

*Corresponding auhor: farnazg@kth.se

†Department of Physics, Ankara University, 06100 Tandoğan, Ankara, Turkey.

‡Deceased.

§Present address: Johannes Gutenberg-Universität Mainz, 55099 Mainz, Germany.

energy of 125 MeV. The experiment was performed at the Grand Accélérateur National d'Ions Lourds (GANIL) in France. The ^{40}Ca beam, provided by the CSSI cyclotron of GANIL, impinged on an (99.83%) isotopically enriched ^{58}Ni target of 6 mg/cm^2 thickness. Prompt γ-ray coincidence events from the reaction products were recorded by the EXOGAM Ge detector array [9] consisting of 11 Compton-suppressed high-purity germanium (HPGe) clover detectors. The detectors were placed in two rings at 90° and 135° relative to the direction of the beam. The Neutron Wall [10] and DIAMANT [11,12] detector arrays were used to observe the coincident emission of neutrons and charged particles, respectively. The Neutron Wall was composed of 50 organic liquid-scintillator detectors covering a 1π solid angle in the forward direction relative to the beam. The DIAMANT detector system, consisting of 80 CsI(Tl) scintillators, was used for detection of evaporated light charged particles with proton- and α-particle efficiencies of 62% and 46%, respectively.

The trigger condition for recording the event data from the experiment was one detected γ ray in any of the Ge clover detectors and a simultaneously detected neutron-like event in the Neutron Wall. This condition was sufficiently relaxed to allow also a fraction of events with no neutrons detected to be recorded, since the hardware gate on the zero-crossover time deduced from the shaping amplifier signals from the neutron detectors accepted a limited number of γ-ray induced signals. In the offline analysis neutron-γ discrimination was performed using two-dimensional cuts on the neutron time of flight versus the zero-crossover time parameters. Selection of the three-proton fusion evaporation reaction channel was performed using the "particle identification" and energy parameters obtained from the DIAMANT detectors. A 50 ns wide time gate was applied to the aligned Ge detector time spectra from EXOGAM in order to ensure prompt coincidences between the detected γ rays. The energy and photopeak efficiency calibration was performed using standard radioactive sources (^{60}Co and ^{152}Eu).

The level scheme of ^{95}Rh (Fig. 1) was deduced from the γ-γ coincidence matrix obtained with the requirement that three protons were detected in DIAMANT. It is also corrected for the "leakage" of events with higher particle multiplicity by subtracting fractions of the corresponding particle-gated matrices. The constructed level scheme confirms to a large extent the previous level scheme as reported in the work by Roth *et al.* [2]. However, in a few instances corrections are introduced. In addition, 20 new transitions involving 15 new excited states are observed in this work. Figure 2 shows examples of coincidence γ-ray energy spectra.

In the positive-parity band six new level energies are added, two levels are removed, the placement of 21 γ-rays is confirmed, and in addition five new transitions are added to the level scheme. The placement of the most of the level energies is in agreement with the level scheme previously reported by Roth *et al.* [2], except for the two observed states at 11 966 and 12 113 keV level energies. Based on the observed coincidences the 12 113 keV level energy was removed and instead a new level at 11 750 keV was confirmed by observing the new, coincident, 885 and 3239 keV transitions which are
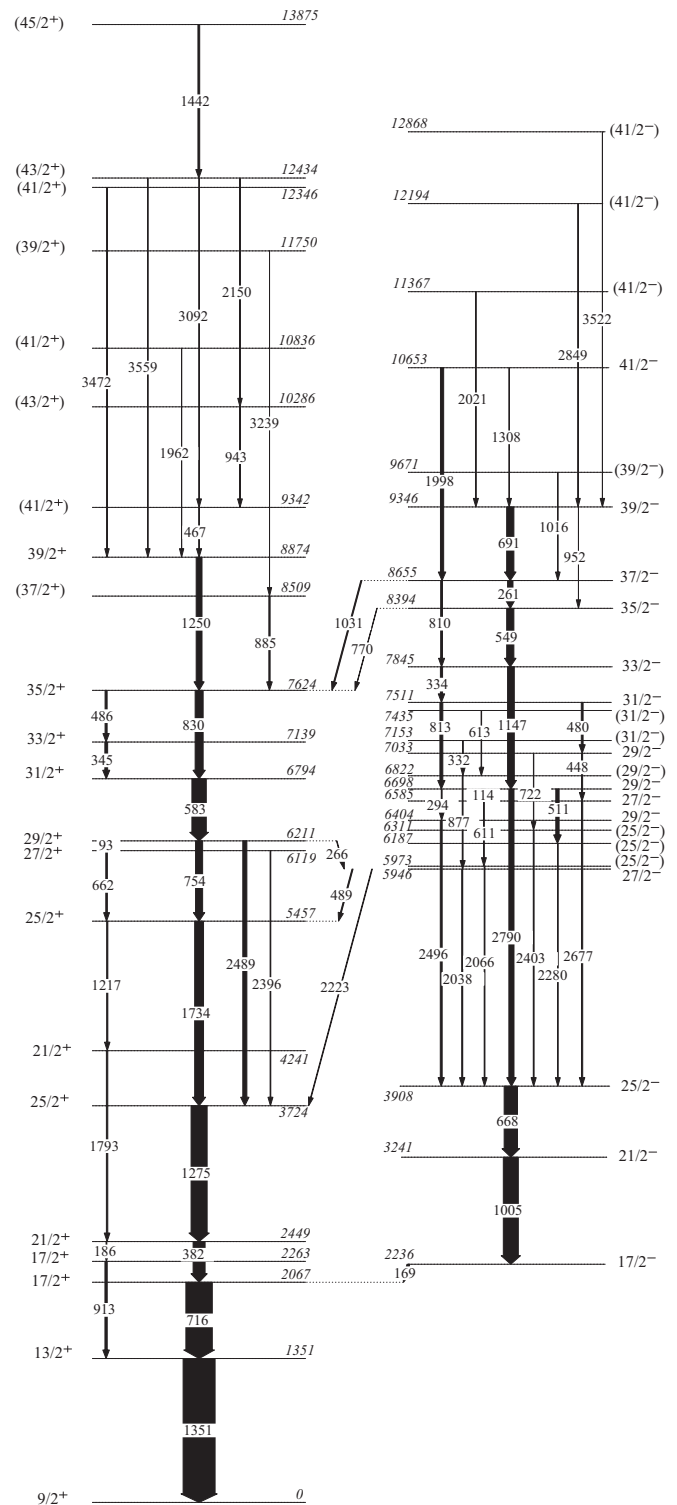

FIG. 1. Partial level scheme of ^{95}Rh. The low energy part, up to $\sim$3 MeV of excitation energy, is identical to the level scheme previously reported in Ref. [2]. The arrows mark the observed γ-ray transitions with their energy given in keV. The widths of arrows are proportional to the measured intensities.

not in coincidence with the 1250 keV transition but are in coincident with the 830 keV transition. The ordering of the 467 and 3092 keV transitions has been reversed based on
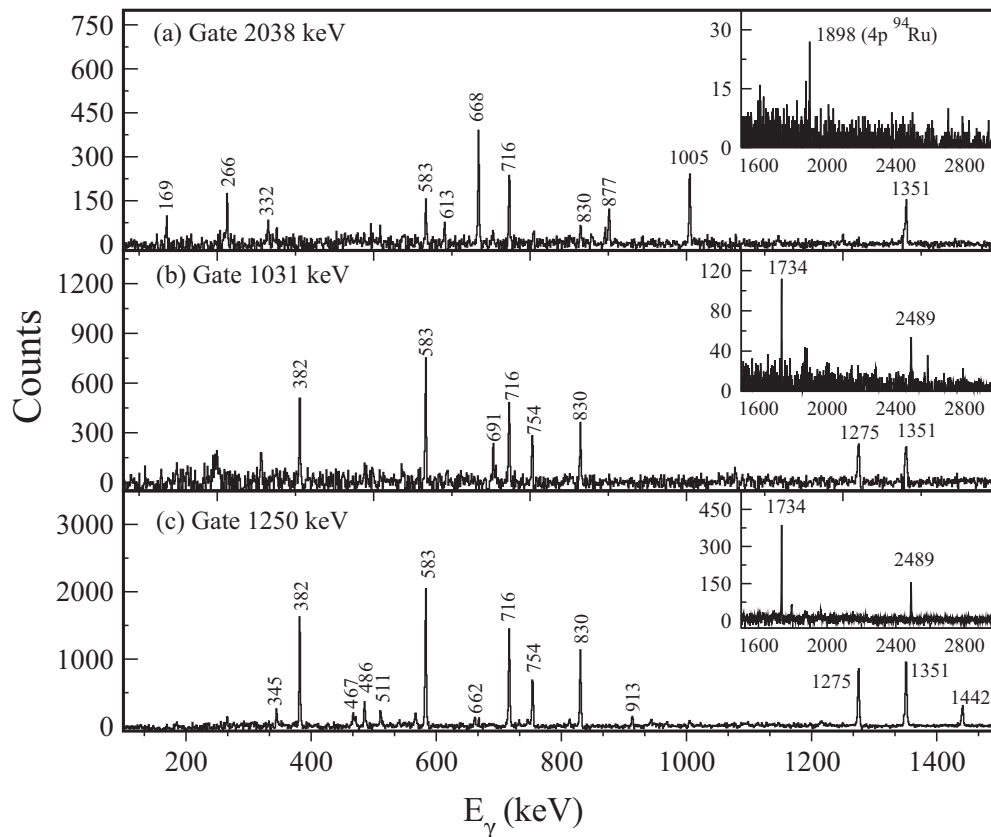
FIG. 2. Gamma-ray coincidence energy spectra gated on the new 2038 keV (a), the 1031 keV (b), and the previously known [2] 1250 keV (c) transitions in ^{95}Rh.

relative intensities, and hence the 11 966 keV level energy was removed and instead a new level was placed at 12 434 keV. Two new transitions, 943 and 2150 keV, were also observed to be in coincidence with the 467 keV transition and were placed in cascade on top of the 9342 keV level. The new 3472 keV transition was observed with the same coincidence pattern as the 3559 keV transition with similar intensity ratios and was, therefore, placed directly above the 1250 keV transition. In the negative-parity band nine new level energies are added, one level is removed, the placement of 20 γ rays is confirmed, and 11 new transitions are added to the level scheme. The ordering of the 448 and 480 keV transitions, which were placed tentatively in Ref. [2], was reversed by observing a new level at 6311 keV and two new connecting transitions, 721 and 2403 keV, in coincidence with the 480 keV transition. A new level at 5946 keV excitation energy was observed with two new feeding transitions and three new transitions depopulating it. The spin-parity assignments for some of the strongest populated states were deduced in this work from the combined linear polarization and angular correlation measurements, and they confirm the existence of the two structures with opposite parities, which are connected by several new $E1$ transitions. Due to the low statistics, except for the spin assignment for the $27/2^-_1$ state at 5946 keV, those for the other new levels are tentative. A summary of γ-ray transition energies, asymmetry values (A), R_{DCO} ratios, and spin-parity assignments for ^{95}Rh deduced in this work is given in Table I.

The granularity of the EXOGAM detector array with eight composite clover detectors situated at angles 90° relative to the beam direction makes it a suitable tool to measure linear polarization of γ rays. Defining the emission plane as the plane spanned by the incident beam direction and the direction of the emitted γ ray, the degree of polarization can be determined by measuring the number of Compton scattered events which are scattered parallel ($\phi = 90°$) or perpendicular ($\phi = 0°$) relative to this plane. The relative intensities of γ rays obtained in this way are used to calculate an experimental asymmetry parameter, A, which is proportional to the degree of linear polarization (normalized to the corrected total intensity). The asymmetry parameter is defined as

$$A = \frac{a(E_\gamma)I_{90°} - I_{0°}}{a(E_\gamma)I_{90°} + I_{0°}}. \tag{1}$$

Here we use a scaling factor, $a(E_\gamma)$, related to the geometrical asymmetry of the EXOGAM clovers as deduced in Ref. [13], where also further details of the analysis can be found. The excess polarization spectrum ($I_{90°} - I_{0°}$) for ^{95}Rh is shown in Fig. 3. Assuming that the probability of higher order multipolarities (>2) is negligible, the positive γ-ray peaks correspond to stretched $E1$ or stretched $E2$ radiation and the negative γ-ray peaks correspond to stretched $M1$ radiation. In order to obtain the linear polarization, P, from the measured asymmetry values, the polarization sensitivity factor, Q, of Ref. [14] was used. The spins of excited levels in ^{95}Rh

TABLE I. γ-ray transition energies, asymmetry A, R_{DCO} ratios, and spin-parity assignments in ^{95}Rh. New γ rays or γ rays depopulating states with a different spin-parity assignment compared with Ref. [2] are marked by stars. Statistical uncertainties are given in parenthesis. $\Delta E_\gamma = \pm 0.5$ keV.

E_γ(keV)	Intensity	A	R_{DCO}	$J_i^\pi \rightarrow J_f^\pi$
92.8	84(10)			$29/2^+ \rightarrow 25/2^+$
114.0	107(9)			$29/2_2^- \rightarrow 27/2_2^-$
169.4	82(4)		0.69(1)	$17/2^- \rightarrow 17/2_1^+$
185.7	21(3)		0.74(2)	$21/2_1^+ \rightarrow 17/2_2^+$
261.2	164(5)	$-0.18(8)$	0.69(2)	$37/2^- \rightarrow 35/2^-$
266.2*	16(3)			$29/2^+ \rightarrow 27/2^-$
294.4*	25(3)		0.63(2)	$29/2_2^- \rightarrow 29/2_1^-$
331.8*	8(4)			$(31/2_1^-) \rightarrow (29/2_3^-)$
334.3	67(4)	$-0.14(6)$	0.62(3)	$33/2^- \rightarrow 31/2_3^-$
344.7	86(4)	$-0.14(6)$	0.63(2)	$33/2^+ \rightarrow 31/2^+$
382.4	370(6)	0.01(2)	1.05(2)	$21/2_1^+ \rightarrow 17/2_1^+$
448.5	34(4)			$29/2_4^- \rightarrow 27/2_2^-$
467.4	25(4)			$(41/2_1^+) \rightarrow 39/2_1^+$
479.9	56(4)	$-0.19(6)$	0.62(4)	$31/2_3^- \rightarrow 29/2_4^-$
486.0	63(4)			$35/2^+ \rightarrow 33/2^+$
488.9*	32(4)			$27/2^- \rightarrow 25/2^+$
511.1*	222(5)			$29/2_2^- \rightarrow (25/2_3^-)$
549.3	224(5)	$-0.11(2)$	0.62(1)	$35/2^- \rightarrow 33/2^-$
583.1	448(7)	$-0.09(1)$	0.53(1)	$31/2^+ \rightarrow 29/2^+$
611.0*	19(5)			$27/2_2^- \rightarrow (25/2_2^-)$
613.3*	15(5)			$(31/2_2^-) \rightarrow (29/2_3^-)$
662.1	49(4)	$-0.03(7)$	0.63(5)	$27/2^+ \rightarrow 25/2_2^+$
667.7	416(6)	0.12(1)	0.94(2)	$25/2_1^- \rightarrow 21/2^-$
691.4	225(5)	$-0.13(2)$	0.56(2)	$39/2_1^- \rightarrow 37/2^-$
716.6	825(8)	0.02(1)	1.00(1)	$17/2_1^+ \rightarrow 13/2^+$
721.8*	11(3)			$29/2_4^- \rightarrow (25/2_4^-)$
754.0	221(5)	0.12(2)	1.20(3)	$29/2^+ \rightarrow 25/2_2^+$
770.4	11(3)	$-0.08(14)$	0.97(20)	$35/2^- \rightarrow 35/2^+$
810.0	56(4)			$37/2^- \rightarrow 33/2^-$
813.1	90(4)		0.50(4)	$31/2_3^- \rightarrow 29/2_2^-$
830.4	250(5)	0.09(2)	1.03(3)	$35/2^+ \rightarrow 31/2^+$
876.9*	25(3)			$(29/2_3^-) \rightarrow 27/2_1^-$
884.9*	39(3)			$(37/2^+) \rightarrow 35/2^+$
913.3	71(4)	0.03(4)	0.99(8)	$17/2_2^+ \rightarrow 13/2^+$
942.9*	16(3)			$(43/2_1^+) \rightarrow (41/2_1^+)$
952.2	21(3)			$39/2_1^- \rightarrow 35/2^-$
1005.2	469(7)	0.08(1)	1.04(2)	$21/2^- \rightarrow 17/2^-$
1015.7*	25(3)			$(39/2_2^-) \rightarrow 37/2^-$
1031.1*	33(3)	0.08(9)	0.67(7)	$37/2^- \rightarrow 35/2^+$
1147.4	210(5)	0.07(2)	0.97(2)	$33/2^- \rightarrow 29/2_2^-$
1217.1	36(3)	0.04(10)	0.97(1)	$25/2_2^+ \rightarrow 21/2_2^+$
1250.0	182(5)	0.10(2)	0.96(4)	$39/2_1^- \rightarrow 35/2^+$
1275.0	502(7)	0.14(1)	0.99(4)	$25/2_1^+ \rightarrow 21/2_1^+$
1307.6	10(3)	$-0.16(14)$	0.56(1)	$41/2_1^- \rightarrow 39/2_1^-$
1351.4	1000(9)	0.012(9)	0.97(1)	$13/2^+ \rightarrow 9/2^+$
1441.9	55(3)			$(45/2_1^+) \rightarrow (43/2_2^+)$
1734.4	277(5)	0.11(1)	1.00(2)	$25/2_2^+ \rightarrow 25/2_1^+$
1793.3	43(3)	0.16(7)	1.35(1)	$21/2_2^+ \rightarrow 21/2_1^+$
1962.2*	13(3)			$(41/2_2^+) \rightarrow (39/2^+)$
1997.8	20(2)			$41/2_1^- \rightarrow 37/2^-$
2021.4	24(2)			$(41/2_1^-) \rightarrow (39/2_1^-)$
2038.3*	32(2)	$-0.12(1)$	0.62(6)	$27/2_1^- \rightarrow 25/2^-$
2066.5*	23(2)			$(25/2_2^-) \rightarrow (25/2_1^-)$

TABLE I. (*Continued.*)

E_γ(keV)	Intensity	A	R_{DCO}	$J_i^\pi \rightarrow J_f^\pi$
2149.7*	6(2)			$(43/2_2^+) \rightarrow (43/2_1^+)$
2223.1*	19(2.5)	0.16(1)	0.50(1)	$27/2^- \rightarrow 25/2^+$
2279.8*	18(2.3)			$(25/2_3^-) \rightarrow (25/2_1^-)$
2396.4	21(2.5)			$27/2^+ \rightarrow 25/2_1^+$
2403.3*	25(2.4)			$(25/2_4^-) \rightarrow (25/2_1^-)$
2488.9	127(4)			$29/2^+ \rightarrow 25/2_1^+$
2496.2	59(3)	0.10(4)	1.01(6)	$29/2_1^- \rightarrow 25/2_1^-$
2676.6	38(2)	$-0.07(5)$	0.57(5)	$27/2_2^- \rightarrow 25/2_1^-$
2790.0	160(4)	0.07(2)	0.98(4)	$29/2_2^- \rightarrow 25/2_1^-$
2849.2	5(2)			$(41/2_3^-) \rightarrow 39/2_1^-$
3091.9	15(2)			$(43/2_1^+) \rightarrow (41/2_1^+)$
3239.2	4(1)			$(39/2_1^+) \rightarrow (37/2^+)$
3471.7*	5(1)			$(41/2_1^+) \rightarrow 39/2_1^+$
3521.9	4(1)			$(41/2_4^-) \rightarrow 39/2_1^-$
3559.4	7(1)			$(43/2_2^+) \rightarrow 39/2_1^+$

are assigned based on angular correlation measurements by extracting the experimental angular correlation intensities $I_{\gamma_2\gamma_1}(\theta_1,\theta_2)$ for all possible combinations of detector pairs located at angles θ_1 and θ_2 with respect to the beam. For the EXOGAM array with three detectors at $\theta_1 = 135°$ and eight detectors at $\theta_2 = 90°$, the experimental directional correlations of γ-rays deexciting oriented states, the R_{DCO} ratios, are defined as

$$R_{\mathrm{DCO}} = \frac{I_{\gamma_2}^{\theta_1}(\text{gated by } \gamma_1 \text{ at } \theta_2)}{I_{\gamma_2}^{\theta_2}(\text{gated by } \gamma_1 \text{ at } \theta_1)}, \qquad (2)$$

where $I_{\gamma 1}$ and $I_{\gamma 2}$ are obtained by gating on the corresponding asymmetrical γ-γ coincidences: the 90° versus 135° gated matrix and the 135° versus 90° gated matrix, respectively. By gating on a cleanly separated $E2$ type transition,
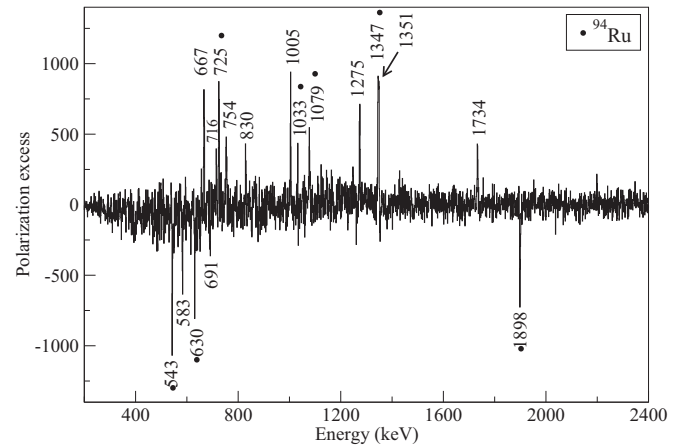

FIG. 3. Polarization measurement for γ rays in ^{95}Rh. The spectrum is selected with a coincidence requirement of three protons detected in the DIAMANT detectors. Gamma-ray lines from the four-proton reaction channel belonging to ^{94}Ru (marked by filled circles) are present due to the limited detection efficiency for protons. See Ref. [13] for details.
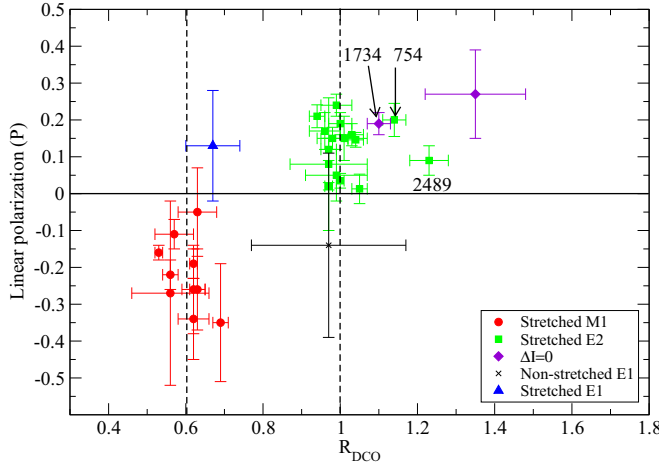
FIG. 4. (Color online) Linear polarization, P, vs angular correlation measurement of γ rays in ^{95}Rh. The stretched $M1$, stretched $E2$, stretched $E1$, and nonstretched $E1$ data points are shown in circles, squares, triangles, and stars, respectively. The color code shows the assigned multipolarity. Blue is stretched $E1$, red is stretched $M1$, green is stretched $E2$, and purple is nonstretched transition ($\Delta I = 0$). A selection of transitions of interest are labeled by their energy values in keV (see text).

γ_1, $R_{\text{DCO}} \sim 0.6$ if γ_2 is a stretched dipole transition and $R_{\text{DCO}} \sim 1$ if γ_2 is a stretched E2 transition [13]. In the present study the R_{DCO} values are obtained by gating on clean $E2$ transitions using the assignments of Ref. [2]. Figure 4 shows the measured linear polarization, P, versus the angular correlation of γ-ray transitions in ^{95}Rh.

III. DISCUSSION

The lowest (yrast) positive parity states in ^{95}Rh, up to $I^\pi = 25/2^+$, can to first order be considered to be built from $\pi(0g_{9/2}^{-5})$ configurations, which can be classified according to their seniority quantum numbers. By including excitations to the neighboring $1p_{1/2}$ as well as the $1p_{3/2}$ and $0f_{5/2}$ orbitals, the accuracy of the calculations of the nuclear wave function may increase [15]. We have first carried out shell model calculations for ^{95}Rh within the restricted model spaces $0g_{9/2}$, $1p_{1/2}0g_{9/2}$, as well as $1p_{1/2}1p_{3/2}0f_{5/2}0g_{9/2}$. The calculations gave very similar results for the excitation energies of the states mentioned above. Our calculations also showed that the inclusion of the $1p_{1/2}$ orbit is essential in reproducing the second $21/2^+$ state at 4241 keV, which is dominated by the configuration $\pi(0g_{9/2}^{-3}1p_{1/2}^{-2})$. For the higher spin excitations shown in Fig. 5, neutron core-excited configurations $[\nu(0g_{9/2}^{-1}1d_{5/2})]$ become important, as suggested in Refs. [2,8] as well as by our LSSM calculations presented below. The yrast negative-parity states, based primarily on $\pi(0g_{9/2}^{-4}1p_{1/2}^{-1})$ configurations, can be constructed in a similar fashion up to the $I^\pi = 25/2_1^-$ state. Most higher-lying negative-parity spin states are also dominated by neutron core excitations, confirming the results of Refs. [2,8,16].

The LSSM calculations performed in this work used $^{100}_{50}$Sn$_{50}$ as a core. We first included the shells $\pi(1p_{1/2}, p_{3/2}, f_{5/2}, g_{9/2})$

(denoted as the fpg model space). The effective interaction matrix elements were taken from Ref. [15].

Figure 5 shows the calculated level energies together with the corresponding experimental data. All states are very well described by the fpg model space up to around 4 MeV of excitation energy. These states can also be nicely reproduced in our calculations in the smaller $0g_{9/2}$ and $1p_{1/2}0g_{9/2}$ model spaces. In general, the structure of ^{95}Rh is very similar to those of the $N = 50$ isotones ^{93}Tc and ^{94}Ru as pointed out in an earlier work [2]. The close resemblance between, for example, the ^{95}Rh and ^{94}Ru level schemes implies that the seniority structures are well preserved. The additional $0g_{9/2}$ proton in ^{95}Rh appears to act mainly as a spectator, and the structure of the low-lying states appears to be quite similar to the corresponding parity states emerging from excitations of six proton holes in the shells $0g_{9/2}$ and $1p_{1/2}$. However, there are clear deviations between the experimentally observed levels and the theoretical prediction using only the fpg model space already for the $25/2_2^+$ and the lowest $27/2^+$, $29/2^+$, and $27/2^-$ states. The calculated $25/2_2^+$ and $27/2_1^+$ states are dominated by the configurations $\pi(1p_{3/2}^{-1}1p_{1/2}^{-1}0g_{9/2}^{-3})$ and $\pi(0f_{5/2}^{-1}1p_{1/2}^{-1}0g_{9/2}^{-3})$, respectively. The theoretically predicted $27/2_1^+$ and $27/2_1^-$ states within the fpg model space are more than 1 MeV higher in excitation energy than the corresponding levels deduced from the experimental data. The predicted $29/2_1^+$ state, which is the highest-spin state one can obtain in the fpg space and which does not appear in calculations in the smaller $0g_{9/2}$ and $1p_{1/2}0g_{9/2}$ model spaces, is 3 MeV higher than the observed $29/2_1^+$ state. This indicates that the influence of other configurations from higher-lying states, beyond the $N = Z = 50$ shell closure, may play an important role here.

The observation of $E1$ transitions in nuclei in this region reveals direct information on the interplay between the deep-lying orbitals $0f_{5/2}$ and $1p_{3/2}$ and the high-lying $0g_{7/2}$ and $1d_{5/2}$ orbitals above the $N = Z = 50$ shell gap. This demonstrates that high-lying single-particle configurations are active, even though the energies of all low-lying states in this region can be well described within the shell model space spanned by the single-particle states $f_{5/2}$, $p_{3/2}$, $p_{1/2}$, and $g_{9/2}$.

The γ-ray branching ratios and previously measured lifetimes of some high-spin states of ^{95}Rh reported in Ref. [8] were used to extract partial decay rates and reduced $E1$ transition probabilities of $E1$ transitions between the positive and negative parity states. The results are shown in Table II.

We estimated the small components of the wave function contributing to the transition probabilities for $E1$ transitions by opening the shells $1d_{5/2}$ and $0g_{7/2}$, which are connected to the deep-lying orbitals $1p_{3/2}$ and $0f_{5/2}$ through the $E1$ operator. Our expanded model space, denoted as $fpgd$, included all orbitals between the $N = Z = 28$ and $N = Z = 64$ subshell closures. The Hamiltonian used here is the same as in our previous work on ^{94}Ru [13] and will therefore only be briefly described here. The two-body interaction matrix elements involving the $0g_{7/2}$ and $1d_{5/2}$ orbitals were derived from the renormalized realistic CD-Bonn nucleon-nucleon potential [17], as in Refs. [18,19]. The effect of core excitation on the low-lying states have been partially taken into account through the renormalization of the two-body interaction,
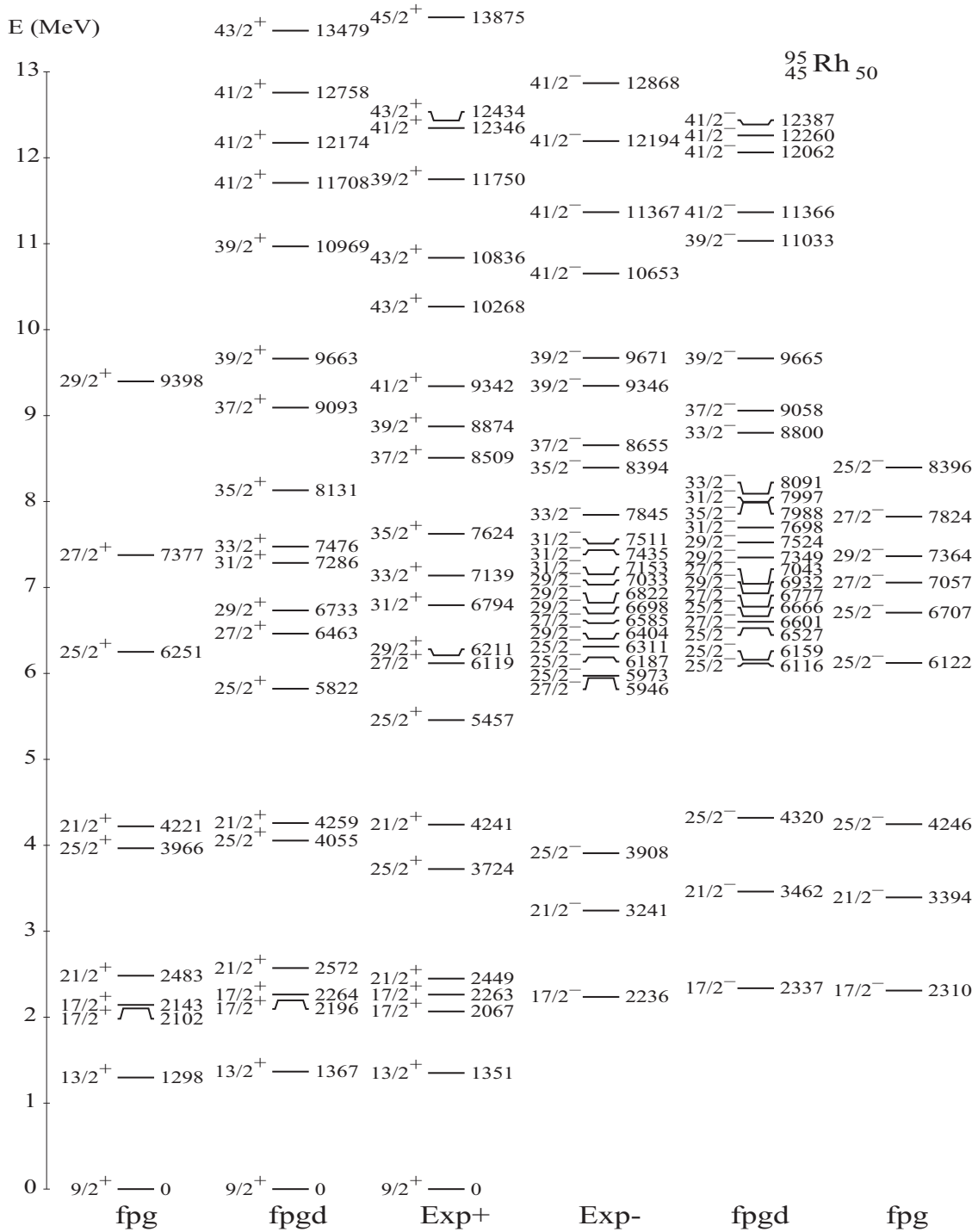
FIG. 5. Comparison between some observed excitation energies and shell model calculations in the fpg and $fpgd$ model spaces for ^{95}Rh.

which is optimized by fitting to experimental data in this region [15]. Therefore, to avoid double counting, we restricted our calculation by allowing at most one particle to be excited from below the $N = 50$ shell gap to the shells above. The single-particle energies of the $0g_{7/2}$ and $1d_{5/2}$ orbitals were determined by fitting to known core-excited states in this region. The results of our calculations in the fpg and $fpgd$ model spaces are shown in Fig. 5. As can be seen from the figure, the results given by the $fpgd$ calculation for low-lying

states up to around 4 MeV are quite similar to those of the fpg model space (as well as to those of the g and pg model spaces not shown here). This indicates that the influence from core excitation on these states is rather limited. The energy of the second $25/2^+$ state is noticeably lower, by about 430 keV, compared with theory. As can be seen from the figure, a good agreement between theory and experiment is achieved up to $I = 37/2$ by simply allowing at most one particle to be excited from below the $N = Z = 50$ shell. These states

TABLE II. The hindrance factors,[a] H, for the observed $E1$ γ-ray transitions as deduced from the branching ratios of this work and lifetimes of the initial states from Ref. [8]. Uncertainties are given in parenthesis. $\Delta E_\gamma = \pm 0.5$ keV.

E_γ (keV)	$J_i^\pi \rightarrow J_f^\pi$	$H \times 10^5$ (W.u.)$^{-1}$
266	$29/2^+ \rightarrow 27/2^-$	0.11(1)
1031	$37/2^- \rightarrow 35/2^+$	0.29(1)
770	$35/2^- \rightarrow 35/2^+$	0.35(1)
169	$17/2^- \rightarrow 17/2_1^+$	2.8(2)

[a]$H = \frac{A^{2/3}}{15.5 \times B(E1)}$.

are dominated by one-neutron core excitation between the $0g_{9/2}$ and $1d_{5/2}$ subshells. An even better agreement can be obtained by lowering the single-particle energies of the $0g_{7/2}$ and $1d_{5/2}$ shells, as mentioned in Ref. [8]. For states with spins higher than 37/2 shown in Fig. 5, many-particle many-hole configurations may become important since the excitation energy is as high as twice the $N = 50$ shell gap. It may also be worthwhile to mention that our calculations do not agree with the predictions in Ref. [8] that the $25/2_2^+$ and $27/2_1^+$ states are dominated by non-core-excitation configurations.

On the negative-parity side, the $25/2_2^-$ and $25/2_3^-$ states calculated in the fpg space, which are separated by around 600 keV, are dominated by the $\pi(1p_{3/2}^{-1}0g_{9/2}^{-4})$ and $\pi(0f_{1/2}^{-1}0g_{9/2}^{-4})$ configurations, respectively. Similarly, the calculated $27/2_1^-$ and $27/2_2^-$ states in the fpg model space are also dominated by the $\pi(1p_{3/2}^{-1}0g_{9/2}^{-4})$ and $\pi(0f_{1/2}^{-1}0g_{9/2}^{-4})$ configurations, respectively. For calculations in the extended $fpgd$ space, it is noticed that the core-excited $25/2_2^-$ state comes lower than the non-core-excited $25/2_3^-$ state, which is dominated by the configuration $\pi(1p_{3/2}^{-1}0g_{9/2}^{-4})$. Both the first and second calculated $27/2^-$ states are dominated by one-neutron core excitation from the shell $0g_{9/2}$ to $1d_{5/2}$. It can be seen from Fig. 5 that a reasonable agreement with experimental data up to the first $39/2^-$ state can be achieved within the $fpgd$ space. A state of particular interest is the new $27/2_1^-$ state mentioned above, which is connected to the $29/2_1^+$, $25/2_2^+$, and $25/2_1^+$ states via stretched $E1$ transitions. A noticeable difference between theory and experiment is seen for this state which is overestimated by about 600 keV and is calculated to be higher than the three lowest $25/2^-$ states. As mentioned before, the low-lying structure of ^{95}Rh is very similar to those of neighboring $N = 50$ isotones. Our calculations show that the structure of the $27/2_1^-$ state in this nucleus can be understood as the coupling of the yrast 13^+ states observed in ^{94}Ru and ^{96}Pd at about 6.6 MeV with the odd proton-hole in the $1p_{1/2}$ orbital.

A critical test of the accuracy of the shell-model wave function may be provided by measurements of $E1$ transition strengths. $E1$ transitions would be strictly forbidden if the model space spanned only the orbitals $g_{9/2}$, $1p_{1/2}$, $0f_{5/2}$, and $1p_{3/2}$ present in the 28–50 shell. This is because the $E1$ transition operator only connects orbitals that differ by orbital angular momentum $\Delta l = 1$ and total angular momentum $\Delta j \leqslant 1$. As mentioned and seen in Fig. 5 of Ref. [2] and

Table II of this work, there are a number of weak $E1$ transitions present, even at low excitation energies (below 5 MeV). We evaluated all possible $E1$ transitions among states within the expanded shell model space. Considering first the $E1$ decay from the first $17/2^-$ state to the yrast $17/2_1^+$ state, these states are predominantly of $\pi(1p_{1/2}^{-1}0g_{9/2}^{-4})$ and $\pi(0g_{9/2}^{-5})$ character, respectively; i.e., without possibility of $E1$ decay. This transition has the largest hindrance, 2.8×10^5 W.u.$^{-1}$ among the $E1$ decays observed in ^{95}Rh which is reflected by the long ($\sim$19 ns) half-life of the $17/2^-$ state [2]. The core-excitation components in these two states are mainly of a one-neutron character. In our calculation the contribution to the transition in terms of occupation probability from the high lying shells $1d_{5/2}$ and $0g_{7/2}$ is 0.02, while the corresponding contribution from the deep-lying shells $1p_{3/2}$ and $0f_{5/2}$ is approximately 10^{-4}. Therefore the $E1$ hindrance factor is of the order 5×10^5 W.u.$^{-1}$, which is consistent with the value given in Table II. The absence of $E1$ transitions depopulating the following negative-parity states up to $25/2^-$ indicates that the influence of the core excited configurations is limited in these states as predicted in Ref. [8]. $E1$ decays observed from the higher-lying negative-parity states as well as from the $29/2_1^+$ state signal significant contributions from core-excited configurations with one neutron being excited from below the $N = 50$ shell closure to the $1d_{5/2}$ or $0g_{7/2}$ orbits, in agreement with the calculations presented in Ref. [20]. The $E1$ transition $29/2^+ \rightarrow 27/2^-$ is observed to be more than 20 times stronger than that of $17/2^- \rightarrow 17/2_1^+$ but is 20 times weaker than that of the $13^+ \rightarrow 12^-$ transition observed in ^{94}Ru [13] even though the $27/2^-$ state has a similar structure to that of the core-excited state 13^+ in ^{94}Ru. This can be understood by the initial $29/2^+$ state also being overwhelmingly dominated by one-neutron core excitation to $1d_{5/2}$, which makes this orbital remain largely inactive during the $E1$ transition process. The enhancement observed in the transition $29/2^+ \rightarrow 27/2^-$ compared to $17/2^- \rightarrow 17/2^+$ is then mainly due to the contribution from the orbitals $0f_{5/2}$ and $0g_{7/2}$.

IV. SUMMARY

Excited states in ^{95}Rh have been studied using the EXOGAM Ge detector array coupled with the Neutron Wall liquid scintillation detector array and the DIAMANT CsI(Tl) charged particle detector system. Directional correlation and polarization measurements enabled unambiguous spin and parity assignments for many of the observed states. The previously reported level scheme was revised and extended and compared with LSSM calculations. $E1$ hindrance factors were deduced from the partial decay rates and used to test the LSSM predictions.

ACKNOWLEDGMENTS

[1] T. Faestermann *et al.*, Prog. Part. Nucl. Phys. **69**, 85 (2013).
[2] H. A. Roth *et al.*, Phys. Rev. C **50**, 1330 (1994).
[3] M. Palacz *et al.*, Phys. Rev. C **86**, 014318 (2012).
[4] M. Lipoglavšek, M. Vencelj, C. Baktash, P. Fallon, P. A. Hausladen, A. Likar, and C.-H. Yu, Phys. Rev. C **72**, 061304 (2005).
[5] M. Gorska *et al.*, Phys. Rev. Lett. **79**, 2415 (1997).
[6] B. Cederwall *et al.*, Nature **68**, 469 (2011).
[7] C. Qi *et al.*, Phys. Rev. C **84**, 021301 (2011).
[8] A. Jungclaus *et al.*, Nucl. Phys. A **637**, 346 (1998).
[9] J. Simpson *et al.*, Acta Phys. Hung. New Ser: Heavy Ion Phys. **11**, 159 (2000).
[10] O. Skeppstedt *et al.*, Nucl. Instrum. Methods A **421**, 531 (1999).
[11] J. N. Scheurer *et al.*, Nucl. Instrum. Methods A **385**, 501 (1997).
[12] J. Gál *et al.*, Nucl. Instrum. Methods A **516**, 502 (2004).
[13] F. Ghazi Moradi *et al.*, Phys. Rev. C **89**, 014301 (2014).
[14] Y. Zheng *et al.*, Phys. Rev. C **87**, 044328 (2013).
[15] M. Honma *et al.*, Phys. Rev. C **80**, 064323 (2009).
[16] I. P. Johnstone and L. D. Skouras, Phys. Rev. C **55**, 1227 (1997).
[17] M. Hjorth-Jensen *et al.*, Phys. Rep. **261**, 125 (1995).
[18] T. Bäck *et al.*, Phys. Rev. C **87**, 031306 (2013).
[19] C. Qi and Z. X. Xu, Phys. Rev. C **86**, 044323 (2012).
[20] K. Muto *et al.*, Phys. Lett. B **135**, 349 (1984).